Optimization of cardiac fiber orientation for homogeneous fiber strain during ejection

Annals of Biomedical Engineering, Vol. 27, pp. 289–297, 1999
Printed in the USA. All rights reserved.

0090-6964/99/27(3)/289/9/$15.00

Optimization of Cardiac Fiber Orientation for Homogeneous Fiber Strain During Ejection

J. RIJCKEN,[1] P. H. M. BOVENDEERD,[2] A. J. G. SCHOOFS,[2] D. H. VAN CAMPEN,[2] and T. ARTS[1]

[1]Department of Biophysics, Cardiovascular Research Institute Maastricht, Maastricht University, Maastricht, The Netherlands and [2]Department of Mechanical Engineering, Eindhoven University of Technology, Eindhoven, The Netherlands

(Received 28 April 1997; accepted 12 February 1999)

Abstract—The strain of muscle fibers in the heart is likely to be distributed uniformly over the cardiac walls during the ejection period of the cardiac cycle. Mathematical models of left ventricular (LV) wall mechanics have shown that the distribution of fiber strain during ejection is sensitive to the orientation of muscle fibers in the wall. In the present study, we tested the hypothesis that fiber orientation in the LV wall is such that fiber strain during ejection is as homogeneous as possible. A finite-element model of LV wall mechanics was set up to compute the distribution of fiber strain at the beginning (BE) and end (EE) of the ejection period of the cardiac cycle, with respect to a middiastolic reference state. The distribution of fiber orientation over the LV wall, quantified by three parameters, was systematically varied to minimize regional differences in fiber shortening during ejection and in the average of fiber strain at BE and EE. A well-defined optimum in the distribution of fiber orientation was found which was not significantly different from anatomical measurements. After optimization, the average of fiber strain at BE and EE was 0.025 $\pm$0.011 (mean$\pm$standard deviation) and the difference in fiber strain during ejection was 0.214$\pm$0.018. The results indicate that the LV structure is designed for maximum homogeneity of fiber strain during ejection. © *1999 Biomedical Engineering Society.* [S0090-6964(99)01603-3]

Keywords—Left ventricle, Finite-element analysis.

INTRODUCTION

Experimental assessment of mechanical load in the cardiac walls, while difficult, indicates spatial homogeneity. Measurement of mechanical load in the form of stress is unreliable because insertion of a force transducer damages the tissue.[18] Strain or segment length has been measured from the relative displacements of markers placed about 5–10 mm apart in the walls of the beating human or canine left ventricle (LV).[3,30,33,41,42] Such measurements indicate that regional differences in fiber strain[12,29,31,42] and in sarcomere length[17] are not significant during the ejection period of the cardiac cycle, with a possible exception at the junction of right and left ventricles.[31] However, the strain measurements are usually restricted to only a few sites in the LV wall.

The spatial distributions of fiber stress and strain in the cardiac walls have also been predicted with mathematical models.[2,5,6,16,19] While some models predict a heterogeneous end-systolic stress distribution,[16] others[6,19,32] indicate that fiber stress during ejection may be quite homogeneous. Moreover, the model studies indicate that the spatial distributions of fiber stress and strain during ejection are sensitive to the transmural course of fiber orientation: with heuristically chosen transmural courses of fiber orientation within the reported anatomical range yielding transmural distributions of fiber stress that were either almost uniform or varied by more than a factor 2. In a recent finite-element model study[32] the spatial distribution of fiber orientation was optimized to give a homogeneous fiber strain distribution at the beginning of ejection. The distribution of fiber orientation thus found was close to reported measurements.[26,37] In that study, only the state of deformation at the beginning of ejection was used as feedback in the optimization. For the transition from diastole to systole, both the passive and active mechanical properties of the tissue are important. To separate the factors related to the active and passive elastic structures, more information is needed about the state of deformation during the cardiac cycle.

In the present study we hypothesized that the distribution of fiber orientation in the LV wall is such that fiber strain during the whole ejection period is as homogeneous as possible. To test the hypothesis a finite-element model of LV wall mechanics was developed to calculate the distribution of fiber stress and strain over the wall at the beginning and end of ejection for a given distribution of fiber orientation. An objective function was defined, expressing the summed inhomogeneity of the average fiber strain at the beginning and end of ejection and of fiber shortening during ejection. In an optimization procedure the objective function was mini-

Address correspondence to T. Arts, Department of Biophysics, Maastricht University, P.O. Box 616, 6200 MD Maastricht, The Netherlands. Electronic mail: T.arts@bf.unimaas.nl

mized by systematic adjustment of the distribution of muscle fiber orientation. The predicted spatial distribution of muscle fiber orientation was compared with anatomical findings. Also, the parameters defining the distribution of fiber orientation were varied over a wide range to study the uniqueness of the calculated optimal distribution of fiber orientation. In subsequent simulations the relative weight of fiber shortening in the objective function was varied to evaluate its effect on the optimal distribution of fiber orientation and on the homogeneity of fiber strain.

METHODS

Finite-Element Model of Left Ventricular Wall Mechanics

The primary setup of the finite-element model has been described before.[32] Changes were made in the description of the distribution of the transverse fiber orientation, and in the active constitutive behavior. The model characteristics are recapitulated below.

Wall Geometry in the Reference State. The reference state for the model was defined as the situation in which transmural pressure and wall stress are 0 kPa. The LV in the reference state was considered thick walled, rotationally symmetric, and point symmetric with respect to the center of the equatorial plane. Midwall geometry was a prolate spheroid. Wall thickness depended on latitude so that base-to-apex gradients in transmurally averaged fiber stresses were minimal. The choice of all model parameter values, including wall geometry dimensions, is given in a separate section below.

Fiber Orientation in Reference State. Fiber orientation in the reference state was quantified by the helix and transverse fiber angles[37] (Fig. 1). The helix fiber angle α_h was defined as the angle between the circumferential direction and the projection of the fiber direction on the plane perpendicular to the regional transmural direction. The transverse fiber angle α_t was defined as the angle between the regional circumferential direction and the projection of the fiber direction on the plane perpendicular to the regional longitudinal direction. The spatial distributions of the helix and transverse fiber angles are specified with respect to a wall-bound coordinate system (u,v). The u coordinate decreases from 0 at the equator to -1 at the apex; the v coordinate is -1, 0, and $+1$ at the endocardial surface, midwall, and epicardial surface, respectively. To describe the distributions of α_h and α_t with as few parameters as possible, we used the following equations:

$$\alpha_h(v) = p_1 + p_2 v, \tag{1}$$

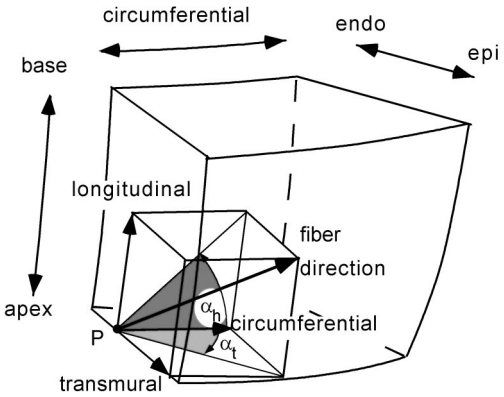

FIGURE 1. Illustration of the helix (α_h) and transverse (α_t) fiber angles in a through-wall block of tissue taken from the left ventricular wall. The fiber angles at a point *P* are defined with respect to the regional transmural, longitudinal, and circumferential directions.

$$\alpha_t(u,v) = p_3 u(1-v^2), \tag{2}$$

where p_1, p_2, and p_3 are parameters whose optimal values are to be determined.

Constitutive Behavior. In the finite-element model, cardiac tissue was considered to consist of stiff fibers embedded in a soft tissue matrix. The total Cauchy stress tensor $\mathbf{T}$ in the tissue is the sum of a passive component $\mathbf{T}_p$ that arises from deformation of passive myocardial tissue and an active component $\mathbf{T}_a$ arising from muscle fiber contraction during systole:

$$\mathbf{T} = \mathbf{T}_p + \mathbf{T}_a . \tag{3}$$

The mechanical behavior of the passive myocardial tissue represents mostly the behavior of the connective tissue and trapped fluid. The passive tissue was assumed capable of bearing a three-dimensional stress that increases exponentially with strain and is zero in the reference state. In accordance with observations[44] the passive tissue was modeled as transversely isotropic, with the stiffness in the fiber direction being twice that in the cross-fiber direction.[32]

The muscle fibers contain sarcomeres, contractile protein units, that are assumed to generate a uniaxial force in the fiber direction during systole. Experimental data on active muscle fiber stress are usually presented as active force per unit undeformed cross-sectional area of the muscle, i.e., in terms of the first Piola–Kirchhoff stress. In the finite-element simulations the first Piola–Kirchhoff active fiber stress T_a^0 (kPa) depended linearly on sarcomere length l_s (μm) and on active stiffness K (kPa):

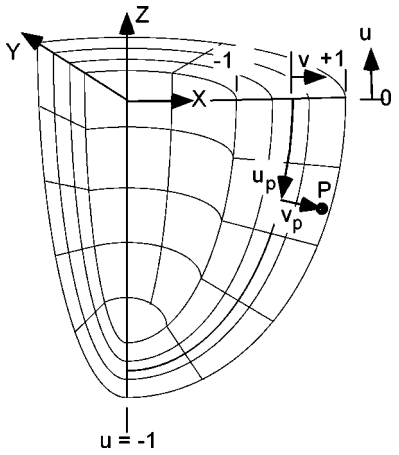

FIGURE 2. Diagram of the rotationally symmetric finite-element mesh of a section of the left ventricular wall between equator and apex. Also shown are: (a) Cartesian coordinate system (X,Y,Z) and (b) wall-bound coordinate system (u,v): point P has coordinates (u_p,v_p). Both u and v vary linearly with distance.

$$T_a^0 = K\frac{l_s - l_x}{l_{s,0}}, \tag{4}$$

where l_x is the sarcomere length at which no contractile force can be generated, and $l_{s,0}$ is the sarcomere length in the reference state. The active stiffness depended on the phase of the cardiac cycle. It was zero in the reference state and during diastole and increased during systole to a maximum value at the end of ejection. The first Piola–Kirchhoff active fiber stress T_a^0 is related to the active stress tensor $\mathbf{T}_a$ by the relation:

$$\mathbf{T}_a = \frac{1}{\det(\mathbf{F})}\mathbf{F}\cdot T_a^0\mathbf{e}_f\mathbf{e}_f, \tag{5}$$

where $\mathbf{F}$ is the deformation gradient tensor,[23] and $\mathbf{e}_f$ is a unit vector in the fiber direction.

Finite-Element Simulations. Calculations of fiber stresses and strains in the LV wall were based on the law of conservation of momentum,[23] expressing static equilibrium of forces in the wall due to both blood pressure in the cavity and internal stresses in the wall. A Galerkin-type finite-element method, implemented in the package DIANA 5.1 (Diana Analysis B.V., Delft, The Netherlands), was used to convert the equations of conservation of momentum into a 20-node three-dimensional brick element formulation with quadratic interpolation of the displacement field. The finite-element mesh comprised the sector of the LV in the region ($X \geqslant 0$, $Y \geqslant 0$, $Z \leqslant 0$) (Fig. 2). The endocardial surface was loaded with LV cavity pressure while the epicardium remained unloaded. Kinematic boundary conditions on the through-wall faces of the mesh allowed cavity volume changes and torsion to occur.

Finite-element simulations started in the reference state of deformation defined above. Cavity pressure and active stiffness were prescribed during the cardiac cycle. The beginning of ejection was defined by a cavity pressure of 12.3 kPa, and an active stiffness of 111.5 kPa corresponding to a cavity-to-wall-volume ratio of approximately 0.65. The end of ejection was defined by a cavity pressure of 17.5 kPa and an active stiffness of 557.7 kPa corresponding to a cavity-to-wall-volume ratio of approximately 0.13.

Quantification of Fiber Strain for Optimization. The LV wall mesh was divided into 729 regions with similar volumes. Sarcomere length at the central point of a region was considered representative for that region. For region i, fiber strain ϵ_i is given by

$$\epsilon_i = \frac{l_{s,i} - l_{s,0}}{l_{s,0}}, \tag{6}$$

where $l_{s,i}$ is the instantaneous sarcomere length in the region and $l_{s,0}$ is the sarcomere length in the reference state.

Optimization Procedure

The optimization consists of the minimization of an objective function G expressing inhomogeneity in fiber strain during ejection:

$$G(\mathbf{p}) = \text{variance}(\epsilon_{\text{be}} + \epsilon_{\text{ee}}) + w \;\; \text{variance}(\epsilon_{\text{be}} - \epsilon_{\text{ee}}), \tag{7}$$

where ϵ_{be} and ϵ_{ee} are fiber strains at the beginning and end of ejection, respectively, and w is a weighting factor. The objective function depends on the fiber orientation parameters p_1, p_2, and p_3 which are stored in the vector $\mathbf{p}$. The contributions of regional fiber strains at the beginning and end of ejection to the variances in Eq. (7) were weighted with the volume of the region. The first variance in Eq. (7) expresses the demand that the average of fiber strain at the beginning and end of ejection be as homogeneous as possible while the second variance demands that fiber shortening be made homogeneous.

To minimize the objective function, the optimization strategy of sequential approximate optimization was used[4] as described previously.[32] Briefly, finite-element analyses are performed for a given set of fiber orientation parameters $\mathbf{p}_k$ to determine the value of the regional fiber strains and their finite-difference first derivatives with respect to $\mathbf{p}$. These values were used to linearly approximate strains ϵ_{be} and ϵ_{ee} near $\mathbf{p}$. The approxima-

tions were substituted in Eq. (7), yielding an analytic approximation function $\hat{G}$, which can be evaluated cheaply. The approximation function is minimized by Powell's method,[28] which is a standard direction-set method for unconstrained optimization of a function. The result of the optimization of $\hat{G}$ is a new set of fiber orientation parameters $\mathbf{p}_{k+1}$.

Convergence was defined to occur when the following two conditions were satisfied. First, finite-element evaluations of the objective function of the current and previous iterations $G(\mathbf{p}_k)$ and $G(\mathbf{p}_{k-1})$, should agree to within a tolerance of δ:

$$[G(\mathbf{p}_{k-1})-G(\mathbf{p}_k)]/G(\mathbf{p}_k)\leqslant\delta, \tag{8}$$

where $\delta=1.0\times10^{-7}$. Second, the minimum of the approximation model based on parameters $\mathbf{p}_k$, $\hat{G}_{\text{opt},\mathbf{p}_k}$ should coincide with the finite-element evaluation of the objective function at $\mathbf{p}_k$, to the same tolerance of δ:

$$[G(\mathbf{p}_k)-\hat{G}_{\text{opt},\mathbf{p}_k}]/G(\mathbf{p}_k)\leqslant\delta. \tag{9}$$

If convergence has not occurred, new approximation models are set up around the parameters $\mathbf{p}_{k+1}$ and the process is repeated.

Applied Parameter Values in Finite-Element Model

Wall Geometry in Reference State. The volume of the model LV wall, extending from the apex to the equator, was 84.1 ml. The volume enclosed by the model LV wall was 25.8 ml. Given that the base of the LV extends above the equator by half the semimajor axis,[39] these volumes are in accordance with measurements in arrested canine ventricles of LV wall mass and cavity volume of 145 ± 19 g (mean$\pm$s.d.), and 40 ± 9 ml, respectively.[24] In the finite-element mesh the ratio of midwall long-to-short axis was set to 2.08.[39] To even out mean-through-wall stresses between equator and apex, the ratio of equatorial-to-apical wall thickness was set to 3.0.

Sarcomere Length in Reference State. In the model, sarcomere length in the reference state $l_{s,0}$ was set to 1.95 μm for all sarcomeres in the LV wall, based on the average of measurements in the left ventricles of rats[15,34] and dogs.[36]

Constitutive Behavior The active material parameter l_x, the zero-force sarcomere length, was set to 1.62 μm, based on experiments in rat cardiac trabeculae.[40] The active stiffness K at end ejection was estimated as 557.7 kPa, from studies in tetanically contracting rat cardiac trabeculae at an external calcium concentration of 2.5 mM.[40] The active stiffness at the beginning of ejection was chosen to be 111.5 kPa so that a cavity pressure of 12.3 kPa resulted in a physiologically realistic cavity volume. The passive material behavior parameters were the same as in Ref. 32.

Performed Simulations

Optimizations were carried out with three different values of the weighting factor w in the objective function of Eq. (7). In the first optimization (optimization REF), the weighting factor was set to unity. Several initial guesses for the parameters (p_1,p_2,p_3) were tried: (0°, −60°, 0°), (−35°, −55°, −30°), (−35°, −55°, 30°), (30°, −60°, 30°), (40°, −50°, −30°), and (40°, −50°, 30°). In two additional optimizations the weighting factor was set to 0.1 and to 10.0, respectively. The initial guess for these optimizations was the best optimum found for the case $w=1.0$. The uniqueness of the optimum was studied for the case $w=1.0$: the objective function was evaluated with the finite-element model for a wide range of the parameters p_1 and p_2 while p_3 was held at its optimal value. Subsequently the objective function was evaluated with p_1 and p_2 set to their optimal values while p_3 was varied.

RESULTS

In optimization REF all the initial guesses resulted in a minimum value of the objective function $G=1.74\times10^{-3}$ [identical to within the tolerance δ of the convergence criterion of Eqs. (8) and (9)]. The optimal fiber orientation parameters were $p_1=20.25°$, $p_2=-65.75°$, and $p_3=16.73°$ (Fig. 3). The corresponding spatial distribution of fiber shortening during ejection and of the average of fiber strain at the beginning and end of ejection is shown in Fig. 4. Despite optimization, large gradients in fiber strains and shortening were observed near the apex. For the quantification of inhomogeneity in fiber strains and shortening, 6% of LV wall volume near the apex was excluded (information from the three elements in the mesh adjoining the apex). The average of fiber strain at the beginning and end of ejection was 0.025 ± 0.011 (mean$\pm$s.d.) while the difference in fiber strain between the beginning and end of ejection was 0.214 ± 0.018 (for the whole LV wall volume these values were 0.023 ± 0.016 and 0.213 ± 0.027, respectively). Extensive variation of helix fiber angle parameters p_1 and p_2 at $p_3=16.73°$ showed that the objective function has at least one other minimum at approximately $p_1=-10°$, $p_2=-15°$, though not as deep as the one that was found in optimization REF (Fig. 5). Variation of transverse fiber angle parameter p_3 at $p_1=20.25°$, $p_2=-65.75°$ indicated that there was only one minimum

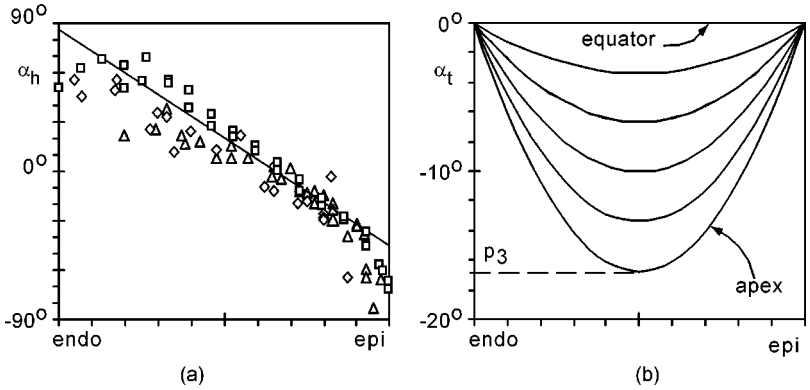

FIGURE 3. (a) Transmural course of helix fiber angle (α_h) after (—) optimization REF. The following measurements are also shown: (□) Streeter (Ref. 37), equatorial region of human LV; (△) Nielsen *et al.* (Ref. 26), equatorial region of canine LV; (◇) Nielsen *et al.* (Ref. 26), adjacent more apical region of canine LV. (b) Transmural course of transverse fiber angle (α_t) at various latitudes ($u = 0.0, -0.2, -0.4, -0.6, -0.8, -1.0$) after optimization REF.

of the objective function, in the same location as the optimized value of $p_3 = 16.73°$ (Fig. 6). Plots similar to Figs. 5(b) and 6 for the separate terms of the objective function G [Eq. (7)], showed the same features as Figs. 5(b) and 6, respectively (not shown). However, inhomogeneity in fiber shortening during ejection was considerably less sensitive to the fiber orientation parameters than inhomogeneity in fiber strain averaged over the beginning and end of ejection.

Tenfold changes in the factor w, weighing the importance of fiber shortening in the objective function of Eq. (7), gave rise to changes of less than ±5% in optimized fiber angle parameters, with respect to values obtained in optimization REF (Table 1). Variation of the weighting factor w gave expected changes in homogeneity of mean-fiber strain and of fiber shortening. Compared to optimization REF, the standard deviation of fiber shortening, $(\epsilon_{be} - \epsilon_{ee})$, decreased for the case $w = 10.0$ and increased for the case $w = 0.1$. Similarly, the standard deviation of the average of fiber strain at the beginning and end of ejection $(\epsilon_{be} + \epsilon_{ee})/2$, increased for the case $w = 10.0$ and decreased for the case $w = 0.1$. For the case $w = 0.1$, the spatial distributions of fiber strain and shortening were almost identical to that for $w = 1.0$ (Fig. 4). Compared to optimization REF, optimization with $w = 10.0$ resulted in fiber strain averages over the beginning and end of ejection that were greater in the endocardial region halfway between equator and apex (not shown).

DISCUSSION

Measurements in normal hearts indicate that regional differences in fiber strain during ejection[12,17,29,31,42] are not significant. Some mathematical models of LV wall mechanics,[2,6,32] but not all,[16] also support the hypothesis of homogeneity of mechanical load. However, myocardial flow in normal hearts appears to be spatially heterogeneous, with the degree of heterogeneity depending inversely on the spatial resolution of the measurements. At a similar resolution to that of strain measurements, flows in the normal baboon LV exhibit a sixfold range and a coefficient of variation of 33%.[20] The apparent discrepancy between the homogeneity of mechanical load and heterogeneity of flow may be partly explained by two

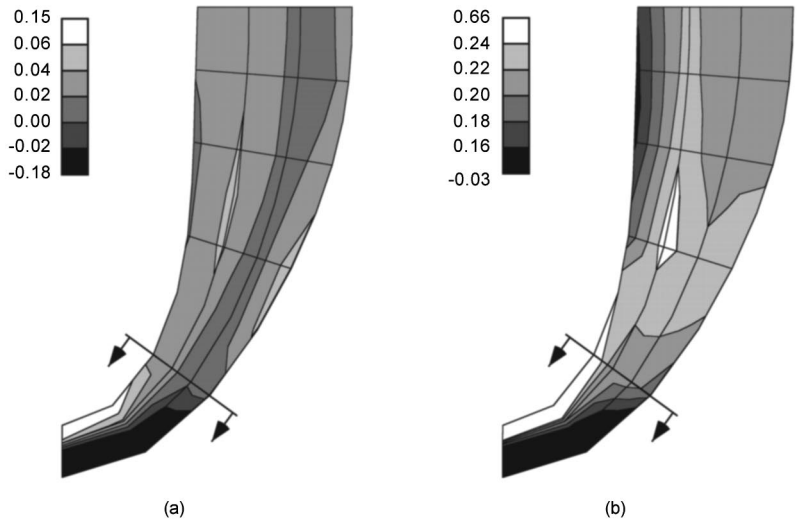

FIGURE 4. Distribution of fiber strain over the LV wall following optimization REF: (a) mean of fiber strain at beginning and end of ejection, $(\epsilon_{be} + \epsilon_{ee})/2$, (b) difference in fiber strain during ejection, $\epsilon_{be} - \epsilon_{ee}$. Owing to the linear relationship between contractile fiber stress and fiber strain, the homogeneity of fiber stress averaged over the beginning and end of ejection is the same as that shown in (a) (under the assumption that stresses during ejection are largely due to contraction). The apical region, indicated by the arrows, was excluded in the quantification of inhomogeneity of fiber strain (see the Results section).

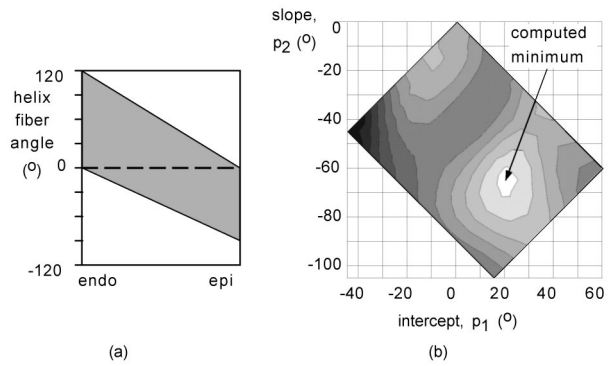

FIGURE 5. Parameter variation of helix fiber angle parameters p_1 and p_2 for the optimized transverse fiber angle parameter ($p_3 = 16.73°$) of optimization REF. The objective function was evaluated with the finite-element model for 130 combinations of p_1 and p_2 in the range indicated by the shaded region in panel (a). Panel (b) shows contour lines along which the objective function value is constant. Contours are drawn at intervals of 2.63×10^{-3}, between 2.63×10^{-3} and 23.67×10^{-3}. The objective function value along the ridge between the two minima is approximately eight times that in the computed minimum.

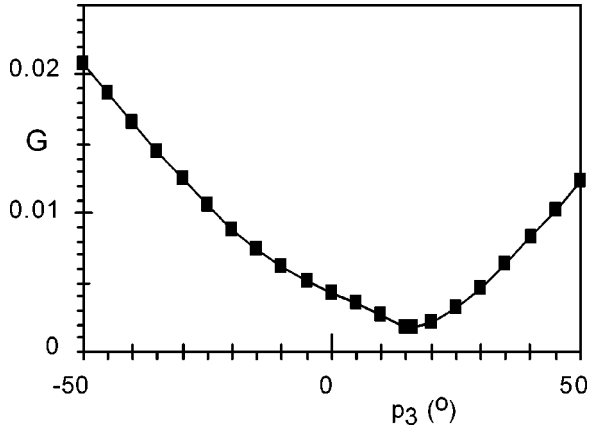

FIGURE 6. Objective function *G* as a function of transverse fiber angle parameter p_3 at optimized values of helix fiber angle parameters ($p_1 = 20.25°$, $p_2 = -65.75°$) for optimization REF. The calculated optimum is at $p_3 = 16.73°$.

factors. First, strain measurements are generally restricted to the LV free wall, a significantly smaller portion of the heart than used in most flow measurements. When flow measurements are restricted to the LV free wall the coefficient of variation decreases to 20%.[14] Second, it is not clear that flow and mechanical load are exactly matched on a regional level. Qualitatively, such a relation has been observed in dog hearts that were paced from various sites. Regions receiving higher flows than the average, also exhibited greater fiber shortening during ejection,[29] and performed more mechanical work.[13] However, quantitative correlations with flow are only moderate for many metabolic variables, such as fatty acid uptake,[35] ATP content, glycogen content,[14] and mitochondrial oxidative capacity.[7] The degree of spatial heterogeneity observed in these metabolic markers is insufficient to explain the spatial variability of flow. Similarly, flow and mechanical load, may not match exactly.

The choice of objective function [Eq. (7)] was based on: (1) measurements that indicate that regional differences in fiber strain during ejection are not significant,[12,17,29,31,42] and (2) experiments in isolated cells[11,43] and in whole hearts[8–10] that indicate that mechanical stimuli are sufficient to give rise to changes in wall mass and structure. These observations suggest that mechanics alone may be the primary determinant of ventricular muscle fiber structure. Minimization of the proposed objective function implies minimization of regional differences in both fiber strain and in fiber strain changes during ejection. The first term of the objective function, the average of fiber strain at the beginning and end of ejection, is also closely related to temporally averaged active fiber stress during ejection. Moreover, the product of temporally averaged fiber stress during ejection and fiber shortening is a good approximation of the external mechanical work that is locally generated. Thus, minimizing the proposed objective function can also be interpreted as minimizing regional differences in external work delivered during ejection.

TABLE 1. Effect of weighting factor w in the objective function minimized [Eq. (7)], on optimized fiber angle parameters p_1, p_2, p_3, and on inhomogeneity of fiber strain. Symbols: ϵ_{be}, ϵ_{ee}=fiber strain at the beginning and end of ejection, respectively. Numbers in parentheses indicate percentage change with respect to REF.

	$w = 0.1$	REF ($w = 1.0$)	$w = 10.0$
p_1 (°)	20.53 (−1.4%)	20.25	19.82 (−2.1%)
p_2 (°)	−66.97 (−1.8%)	−65.75	−62.29 (+5.2%)
p_3 (°)	16.94 (+1.3%)	16.73	16.17 (−3.3%)
mean $[(\epsilon_{be} + \epsilon_{ee})/2]$	0.0256 (+2.1%)	0.0251	0.0233 (−7.2%)
s.d. $[(\epsilon_{be} + \epsilon_{ee}/2)]$	0.010 (−2.5%)	0.011	0.014 (+27.1%)
mean $[\epsilon_{be} - \epsilon_{ee}]$	0.214 (−0.1%)	0.214	0.214 (+0.04%)
s.d. $[\epsilon_{be} - \epsilon_{ee}]$	0.019 (+6.1%)	0.018	0.016 (−10.4%)

For simplicity, residual strain has not been included in the finite-element model. Measurements indicate that circumferential residual strain leads to a transmural gradient in sarcomere length in the unloaded left ventricle of the rat.[34] At positive filling pressure the transmural gradient in sarcomere length becomes less pronounced, indicating that residual strain may contribute to homogeneity of fiber strain at the beginning of ejection.[15] However, finite-element simulations of LV wall mechanics show that the effects of residual strain, represented by a transmural gradient in sarcomere length in the zero-pressure reference state, do not affect the end-systolic distribution of fiber strain.[16]

For reasons of simplicity we have also not incorporated recent data[21,22] showing that the muscle fibers are arranged in collagen-connected sheets of about 4 muscle cells thick. The sheets tend to be arranged in a transmural direction in the middle of the LV wall and more tangential to the wall at the inner and outer surfaces. According to these data the mechanical properties of a piece of myocardium depend not only on the orientation of the muscle fibers, as is assumed in the present study, but also on the orientation of the fiber sheets.

A limitation of the present study is that we did not change the size of the elements in the finite-element mesh of the LV wall to check the stress, strain, or displacement convergence of the finite-element solution. However, for a transmural course of helix fiber angle according to measurements,[38] the distributions of sarcomere length and fiber stress were similar to those computed by an independently developed finite-element model of LV wall mechanics.[19]

The finite-element model of LV wall mechanics in the present study is most representative of the mechanics of the LV free wall. The base of the LV wall was not included to avoid problems in specifying appropriate boundary conditions, representing the action of the annulus fibrosis. Others[6,19] have found that imposing purely kinematic boundary conditions at the base can lead to unrealistic stress distributions. To avoid problems in specifying boundary conditions at the base only the region between the equator and apex was modeled. Suitable boundary conditions for the equator could be derived on the basis of point symmetry with respect to the center of the equatorial plane. The apex was included in the present finite-element model but we recognize that the description of its mechanics is probably erroneous due to an inadequate description of its fiber orientation, wall geometry, and material properties. After all, the apex is a singular point in the mathematical description of the distribution of fiber orientation. Hence, while fiber orientation was optimized in the whole LV wall mesh, mean and standard deviation values over the wall have been calculated without information from the three elements (comprising 6% of LV wall volume) adjoining the apex.

In the optimization strategy used in this study the obtained minimum may depend on the initial guess of the fiber orientation parameters. To investigate whether there were other minima in the neighborhood of the computed minimum, the objective function was evaluated over a wide range of the fiber orientation parameters. From the parameter variation, it can be concluded that for a given value of the transverse fiber angle parameter of $p_3 = 16.73°$, the helix fiber angle parameters resulting from the standard optimization REF give the lowest minimum in objective function [Fig. 5(b)]. Furthermore, for given helix fiber angle parameters of $p_1 = 20.25°$, $p_2 = -65.75°$ the transverse fiber angle parameter resulting from optimization REF gives the lowest minimum (Fig. 6). Figures 5 and 6 show that the computed minimum of the objective function is well defined; there are no other local minima visible in the close neighborhood. Although not proved, the performed parameter variation indicates it is likely that the computed minimum is the lowest minimum in the anatomical range.

Despite optimization of fiber orientation, fiber shortening during ejection varies between approximately 0.15 and 0.23 near the equator [Fig. 4(b)], which is still considerable. It is to be expected that this range will narrow when allowing a more detailed description of the global fiber structure in the LV wall by using more fiber orientation parameters. For the whole, LV fiber shortening during ejection is 0.214 ± 0.018, which is rather large but not abnormal. Measurements in the dog heart show that fiber shortening during ejection is typically 0.3 μm,[33] or ranges between 0.2 and 0.4 μm.[17] The choice of ejection fraction in the simulations is not expected to significantly affect the optimization results and the conclusions of the study.

In a previous effort to compute the fibrous structure of the LV, a similar finite-element model was used to optimize the distribution of fiber orientation for homogeneous fiber strain at the beginning of ejection.[32] The helix fiber angle distribution was defined by the same parameters $p1$ and $p2$. The transverse fiber angle varied sinusoidally with longitude (u), rather than linearly as in the current study. Their optimized values were $(p_1, p_2, p_3) = (21.0°, -69.2°, 15.3°)$, which is similar to those found here. The main advance of the current study is that the optimization includes strain information from a larger part of the ejection period. Also, in the current study the contractile behavior has been modeled more accurately. Finally, in the current study the sensitivity of the results to various model parameters (Table 1, Figs. 5 and 6) has been investigated more thoroughly.

To assess the transmural course of helix fiber angle, comparisons were made with reported measurements in

the equatorial region of the human LV[37] and in equatorial and adjacent more apical regions of the canine LV.[26] The computed transmural course of helix fiber angle lies within the measured range of helix fiber angles over the majority of the wall thickness (Fig. 3). For a quantitative comparison, the root-mean-squared (rms) difference between the computed transmural course of helix fiber angle and several measurement series was determined. The rms differences were $\pm 11.9°$ and $\pm 17.3°$ for measurements at the equator by Streeter[37] and Nielsen *et al.*,[26] respectively, and $\pm 15.1°$ closer to the apex.[26] Best linear fits to each of the measurement series had rms differences ranging from $\pm 11.4°$ to $\pm 12.1°$, which are only slightly smaller than rms differences between the measured and predicted transmural course. The rms differences found in this study for the optimized distribution of fiber orientation are similar to those found in other models.[1,6,27,32] In summary, both qualitative and quantitative comparisons of the computed transmural course of helix fiber angle with measurements indicate that the predicted helix angle is not significantly different from the measurements.

Assessment of the computed distribution of transverse fiber angle is difficult due to the scarcity of other data. Mean-through-wall values have been measured as $-4.6 \pm 0.8°$ (mean$\pm$sem, $n=12$) near the equator and $-3.5 \pm 0.6°$ ($n=15$) near the apex.[37] In our model the spatial average of α_t below the equator is $-5.6°$ which is not in contradiction with these measurements, and similar to previous model predictions.[32] In an independent mathematical model to calculate left ventricular fiber orientation,[27] the transverse fiber angle was zero at the wall surfaces and greatest in the middle of the wall. The midwall transverse fiber angle decreased from 0° at the equator to approximately $-18°$ at a position corresponding to $u=-0.75$. At this position we predict a transverse angle of $-12.5°$. In conclusion, only limited information is available for quantitative evaluation of the computed transverse fiber angle. Our predictions do not conflict with this information.

Conclusions on the basis of the present study regarding a mechanism for cardiac adaptation must be considered with caution. Our results support the hypothesis that fibers are oriented in the LV wall such that fiber strain during ejection is as homogeneous as possible. However, the applied optimization strategy, in which information about fiber strain from all over the LV wall is used to adapt regional fiber orientation, is unlikely to be the basis of a physiological adaptation mechanism. Cardiac adaptation is more likely to be controlled in the environment of the cell,[1] as has also been proposed for bone adaptation.[25]

In conclusion, an objective function expressing inhomogeneity of fiber strain averaged over the beginning and end of ejection and inhomogeneity of fiber shortening during ejection has been minimized by optimization of fiber orientation. A well-defined minimum in the objective function was found for which mean-fiber strain during ejection and the difference in fiber strain between the beginning and end of ejection were 0.025 ± 0.011 (mean$\pm$s.d.) and 0.214 ± 0.018, respectively. After optimization the helix fiber angle varied from 86.0° at the endocardium to $-45.5°$ at the epicardium. Comparison with anatomical measurements shows that the optimized transmural course of the helix fiber angle is not significantly different. Moreover, the optimizations predict that fibers have a significant transmural component, quantified by the transverse angle, with a spatial average between equator and apex of $-5.6°$. The results indicate that the structure of the left ventricle is designed for maximum homogeneity of fiber strain during ejection.

REFERENCES

[1] Arts, T., F. W. Prinzen, L. H. E. H. Snoeckx, J. M. Rijcken, and R. S. Reneman. Adaptation of cardiac structure by mechanical feedback in the environment of the cell: A model study. *Biophys. J.* 66:953–961, 1994.

[2] Arts, T., and R. S. Reneman. Dynamics of left ventricular wall and mitral valve mechanics—A model study. *J. Biomech.* 22:261–271, 1989.

[3] Azhari, H., J. L. Weiss, W. J. Rogers, C. O. Siu, E. A. Zerhouni, and E. P. Shapiro. Noninvasive quantification of principal strains in normal canine hearts using tagged MRI images in 3-D. *Am. J. Physiol.* 264:H205–H216, 1993.

[4] Barthelemy, J.-F. M., and R. T. Haftka. Approximation concepts for optimum structural design—A review. *Struct. Optim.* 5:129–144, 1993.

[5] Beyar, R., and S. Sideman. Left ventricular mechanics related to the local distribution of oxygen demand throughout the wall. *Circ. Res.* 58:664–677, 1986.

[6] Bovendeerd, P. H. M., T. Arts, J. M. Huyghe, D. H. van Campen, and R. S. Reneman. Dependence of local left ventricular wall mechanics on myocardial fiber orientation: A model study. *J. Biomech.* 25:1129–1140, 1992.

[7] Bussemaker, J., J. H. G. M. van Beek, A. B. J. Groeneveld, M. Hennekes, T. Teerlink, L. G. Thijs, and N. Westerhof. Local mitochondrial enzyme activity correlates with myocardial blood flow at basal workloads. *J. Mol. Cell. Cardiol.* 26:1017–1028, 1994.

[8] Carew, T. E., and J. W. Covell. Fiber orientation in the hypertrophied canine left ventricle. *Am. J. Physiol.* 236:H487–H493, 1979.

[9] Cooper IV, G. Cardiocyte adaptation to chronically altered load. *Annu. Rev. Physiol.* 49:501–518, 1987.

[10] Cooper IV, G., R. L. Kent, C. E. Uboh, E. W. Thompson, and T. A. Marino. Hemodynamic versus adrenergic control of cat right ventricular hypertrophy. *J. Clin. Invest.* 75:1403–1414, 1985.

[11] Cooper IV, G., W. E. Mercer, J. K. Hoober, P. R. Gordon, R. L. Kent, I. K. Lauva, and T. A. Marino. Load regulation of the properties of adult feline cardiocytes: The role of substrate adhesion. *Circ. Res.* 58:692–706, 1986.

[12] Delhaas, T., T. Arts, P. H. M. Bovendeerd, F. W. Prinzen, and R. S. Reneman. Subepicardial fiber strain and stress as

related to left ventricular pressure and volume. *Am. J. Physiol.* 264:H1548–H1559, 1993.
[13] Delhaas, T., T. Arts, F. W. Prinzen, and R. S. Reneman. Regional fiber stress-fiber strain area as estimate of regional oxygen demand in the canine heart. *J. Physiol. (London)* 477:481–496, 1994.
[14] Franzen, D., R. S. Conway, H. Zhang, E. H. Sonnenblick, and C. Eng. Spatial heterogeneity of local blood flow and metabolite content in dog hearts. *Am. J. Physiol.* 254:H344–H353, 1988.
[15] Grimm, A. H., H.-L. Lin, and B. R. Grimm. Left ventricular free wall and intraventricular pressure-sarcomere length distributions. *Am. J. Physiol.* 239:H101–H107, 1980.
[16] Guccione, J. M., K. D. Costa, and A. D. McCulloch. Finite element stress analysis of left ventricular mechanics in the beating dog heart. *J. Biomech.* 28:1167–1177, 1995.
[17] Guccione, J. M., W. G. O'Dell, A. D. McCulloch, and W. C. Hunter. Anterior and posterior left ventricular sarcomere lengths behave similarly during ejection. *Am. J. Physiol.* 272:H469–H477, 1997.
[18] Huisman, R. F., G. Elzinga, N. Westerhof, and P. Sipkema. Measurement of ventricular wall stress. *Cardiovasc. Res.* 14:142–153, 1980.
[19] Huyghe, J. M., T. Arts, D. H. van Campen, and R. S. Reneman. Porous medium finite element model of the beating left ventricle. *Am. J. Physiol.* 262:H1256–H1267, 1992.
[20] King, R. B., J. B. Bassingthwaighte, J. R. S. Hales, and L. B. Rowell. Stability of heterogeneity of myocardial blood flow in normal awake baboons. *Circ. Res.* 57:285–295, 1985.
[21] LeGrice, I. J., P. J. Hunter, and B. H. Smaill. Laminar structure of the heart: A mathematical model. *Am. J. Physiol.* 272:H2466–H2476, 1997.
[22] LeGrice, I. J., B. H. Smaill, L. Z. Chai, S. G. Edgar, J. B. Gavin, and P. J. Hunter. Laminar structure of the heart: Ventricular myocyte arrangement and connective tissue architecture in the dog. *Am. J. Physiol.* 269:H571–H582, 1995.
[23] Malvern L. E. Introduction to the Mechanics of a Continuous Medium. London: Prentice-Hall, 1969.
[24] McCulloch, A. D., B. H. Smaill, and P. J. Hunter. Regional left ventricular epicardial deformation in the passive dog heart. *Circ. Res.* 64:721–733, 1989.
[25] Mullender, M. G., R. Huiskes, and H. Weinans. A physiological approach to the simulation of bone remodeling as a self-organizational control process. *J. Biomech.* 27:1389–1394, 1994.
[26] Nielsen, P. M. F., I. J. Le Grice, B. H. Smaill, and P. J. Hunter. Mathematical model of geometry and fibrous structure of the heart. *Am. J. Physiol.* 260:H1365–H1378, 1991.
[27] Peskin, C. S. Fiber architecture of the left ventricular wall: An asymptotic analysis. *Commun. Pure Appl. Math.* 42:79–113, 1989.
[28] Press, W. H., B. P. Flannery, S. A. Teukolsky, and W. T. Vetterling. Numerical Recipes. The Art of Scientific Computing. Cambridge: Cambridge University Press, 1986.
[29] Prinzen, F. W., C. H. Augustijn, T. Arts, M. A. Allessie, and R. S. Reneman. Redistribution of myocardial fiber strain and blood flow by asynchronous electrical activation. *Am. J. Physiol.* 259:H300–H308, 1990.
[30] Prinzen, T. T., T. Arts, F. W. Prinzen, and R. S. Reneman. Mapping of epicardial deformation using a video processing technique. *J. Biomech.* 19:263–273, 1986.
[31] Rademakers, F. E., W. J. Rogers, W. H. Guier, G. M. Hutchins, C. O. Siu, M. L. Weisfeldt, J. L. Weiss, and E. P. Shapiro. Relation of regional cross-fiber shortening to wall thickening in the intact heart. Three-dimensional strain analysis by NMR tagging. *Circulation* 89:1174–1182, 1994.
[32] Rijcken, J., P. H. M. Bovendeerd, A. J. G. Schoofs, D. H. van Campen, and T. Arts. Optimization of cardiac fiber orientation for homogeneous fiber strain at beginning of ejection. *J. Biomech.* 30:1041–1049, 1997.
[33] Rodriguez, E. K., W. C. Hunter, M. J. Royce, M. K. Leppo, A. S. Douglas, and H. F. Weisman. A method to reconstruct myocardial sarcomere lengths and orientations at transmural sites in beating canine hearts. *Am. J. Physiol.* 263:H293–H306, 1992.
[34] Rodriguez, E. K., J. H. Omens, L. K. Waldman, and A. D. McCulloch. Effect of residual stress on transmural sarcomere length distributions in rat left ventricle. *Am. J. Physiol.* 264:H1048–H1056, 1993.
[35] Sloof, G. W., F. C. Visser, E. F. I. Comans, A. B. J. Groeneveld, J. J. Bax, M. J. van Eenige, G. J. van der Vusse, and F. F. J. Knapp. Heterogeneity of DMIPP uptake and its relationship with heterogeneous myocardial blood flow. *J. Nucl. Med.* 38:1424–1430, 1997.
[36] Spotnitz, H. M., E. H. Sonnenblick, and D. Spiro. Relation of ultrastructure to function in the intact heart: Sarcomere structure relative to pressure volume curves of intact left ventricles of dog and cat. *Circ. Res.* 18:49–66, 1966.
[37] Streeter, Jr., D. D. Gross morphology and fiber geometry of the heart. In: Handbook of Physiology—The Cardiovascular System I, edited by R. M. Berne. Bethesda, MD: Am. Physiol. Soc., 1979, pp. 61–112.
[38] Streeter, Jr., D. D., H. M. Spotnitz, D. P. Patel, J. Ross, Jr., and E. H. Sonnenblick. Fiber orientation in the canine left ventricle during diastole and systole. *Circ. Res.* 24:339–347, 1969.
[39] Streeter, D. D. J., and W. T. Hanna. Engineering mechanics for successive states in canine left ventricular myocardium. 1. Cavity and wall geometry. *Circ. Res.* 33:639–655, 1973.
[40] ter Keurs, H. E. D., W. H. Rijnsburger, R. van Heuningen, and M. J. Nagelsmit. Tension development and sarcomere length in rat cardiac trabeculae: Evidence of length-dependent activation. *Circ. Res.* 46:703–714, 1980.
[41] Villarreal, F. J., and W. Y. W. Lew. Finite strains in anterior and posterior wall of canine left ventricle. *Am. J. Physiol.* 259:H1409–H1418, 1990.
[42] Waldman, L. K., D. Nosan, F. Villarreal, and J. W. Covell. Relation between transmural deformation and local myofiber direction in canine left ventricle. *Circ. Res.* 63:550–562, 1988.
[43] Watson, P. A. Function follows form: Generation of intracellular signals by cell deformation. *FASEB J.* 5:2013–2019, 1991.
[44] Yin, F. C. P., R. K. Strumpf, P. H. Chew, and S. L. Zeger. Quantification of the mechanical properties of noncontracting canine myocardium under simultaneous biaxial loading. *J. Biomech.* 20:577–589, 1987.